Mechanism and Machine Theory 190 (2023) 105445

Contents lists available at ScienceDirect

Mechanism and Machine Theory

journal homepage: www.elsevier.com/locate/mechmt

Review

Kinematic properties of nth—order Bresse circles intersections for a crank-driven rigid body

Giorgio Figliolini [a,*], Chiara Lanni [a], Marco Cirelli [b], Ettore Pennestrì [b]

[a] *DICEM, University of Cassino & Southern Lazio, Via G. Di Biasio 43, Cassino (FR) 03043, Italy*
[b] *Department of Enterprise Engineering, University of Rome Tor Vergata, Via del Politecnico 1, Roma 00133, Italy*

ARTICLE INFO

Keywords:
Higher-order planar kinematics
Crank-driven rigid body
nth-order poles and Bresse circles
Four-bar kinematic chain
Higher-order path curvature analysis

ABSTRACT

This paper is focused on higher-order planar kinematics and deals with the kinematic properties of the nth-order poles and Bresse circles intersections for a crank-driven rigid body, which belongs to a four-bar kinematic chain in the form of a four-bar, a slider-crank or a swinging-block mechanism. In particular, specific kinematic properties of nth-order Bresse circles are presented and proven for the first time in the form of three novel theorems, by means of the proposed formulation, which has been validated by significant graphical and numerical results for several crank-driven four-bar mechanisms in different configurations.

1. Introduction

The kinematic analysis of planar mechanisms can be developed by means of both graphical and analytical methods, as widely described in several text books [1–4]. Currently, the traditional graphical methods are applied by using two-dimensional CAD systems or solid modeling systems, while the analytical methods can be found in commercially available programs or specific user-written computer programs in a high-level language can be created.

The kinematic analysis is usually developed up to the accelerations, but there are many practical applications where it is necessary to increase the order of the time-derivative of the position vector of a generic particle or rigid body point. In particular, the jerk is quite common for the kinematic synthesis and analysis of indexing mechanisms with cams or Geneva wheels, because the cam profile and the curved slots are very sensitive to the assigned motion program, which gives the maximum jerk values, as discussed in [5].

Other examples regard the kinematic performance of long-dwell mechanisms, which are designed by applying the dead-point superposition method and thus obtaining dead-points with zero jerk or jounce, as reported in [6]. Consequently, the dynamical performance of a mechanical system depends by the inertia forces, which are related to the accelerations, while the shock-loading problems are jerk dependent and sometime, even the jounce or the displacement fourth time-derivative is convenient to be considered, in order to obtain a smooth motion, without impulsive dynamic loads.

Moreover, these kinematic and dynamic properties are also strictly related to the differential geometry and curvature theory, because the successive time-derivatives of a particle position vector, give in sequence, the velocity, acceleration, jerk, jounce, etc. vectors, which can be also decomposed in their components on the local and moving Frenet-Serret frame, as analyzed in [7–9] for the Euclidean 3-space. In fact, these components have more physical meaning since depending by both variations of the magnitude and

* Corresponding author.
E-mail addresses: figliolini@unicas.it (G. Figliolini), lanni@unicas.it (C. Lanni), marco.cirelli@uniroma2.it (M. Cirelli), pennestri@mec.uniroma2.it (E. Pennestrì).

https://doi.org/10.1016/j.mechmachtheory.2023.105445
Received 17 February 2023; Received in revised form 19 July 2023; Accepted 19 July 2023

orientation of each kinematic vector. These properties were extended by the particle to the planar or spatial rigid body motion with the aid of the screw-theory in terms of twist and wrench, as proposed in [10–12].

The motion program is usually assigned in the form of the acceleration diagram, which can be constant, simple harmonic, cycloidal or polynomial, but focusing on the displacement higher-order time-derivatives, as the jerk and jounce, other more suitable motion programs can be defined, as reported in [13], where the case of the elliptic jerk diagram was considered to derive those of the acceleration, velocity and displacement by successive integration. According to this approach, another application can be found in [14], where it was observed that the vibration of CNC machines decreases significantly for motions under confined jounce than those under confined acceleration and jerk, and in [15], where the importance of jerk analysis was investigated for the case of structural dynamics. A novel application regarding the analysis of the angular head jerk in augmented and virtual reality is also reported in [16].

In particular, the kinematic analysis of planar mechanisms that makes use of Bresse's circles is less common, especially when they are computed and plotted by making use of the computer, even if, they provide a better physical understanding of the motion, along with its velocity and acceleration vector fields, as first proposed in [17]. In fact, these geometric loci intersect each other at both centers or poles of the instantaneous rotation and acceleration, which are also the centers of two corresponding vector fields, as widely analyzed in [18–23]. More recently, some properties of higher order instant centers and a new graphical technique for the acceleration analysis of four-bar mechanisms were reported in [24] and [25]. An extension of this approach to the endless tendon driven mechanisms was proposed in [26], while the application to the spherical case, can be found in [27,28] and other dealing with the geometric loci, in terms of inflection circle and centrodes, are reported in [29–31]. The synthesis of quasi-constant transmission ratio planar linkages was proposed in [32].

A first formulation based on the instantaneous geometric invariants was proposed in [33] to obtain the first and second order centrodes of eccentric slider-crank mechanisms. The Bresse circles were also included in the proposed algorithm, in order to validate the right positions of both instantaneous center of rotation and acceleration pole of the coupler link. Moreover, a pure geometrical approach was applied to centered slider-crank mechanisms in [34] by using the Euler-Savary equation and the Bresse and jerk circles were obtained.

This paper is focused on higher-order planar kinematics and deals with the kinematic properties of the n^{th}-order poles and Bresse circles intersections for a crank-driven rigid body, which belongs to a four-bar kinematic chain in the form of a four-bar, a slider-crank or a swinging block mechanism and thus, the previous algorithm was reformulated and extended.

In particular, the classic Bresse circles are the loci of points with zero tangential and normal acceleration, respectively. The following properties are observed:

- the circles intersect[1] at velocity and acceleration poles P_1 and P_2;
- the tangents to the circles at intersection points are perpendicular.

Since the classic Bresse cicles represent the field of acceleration in a planar motion, herein it is proposed to denote them as 2nd-order Bresse circles. For the 3rd-order kinematic analysis one can introduce the jerk circles, as reported in [2,3,34], i.e. the loci of moving points with zero tangential and normal jerk.

For these loci circles, the following properties are observed:

- the circles intersect[2] at velocity and jerk poles P_1 and P_3;
- the tangents to the circles at intersection points are perpendicular.

Due to the striking similarity of properties shared with classic Bresse circles, the jerk circles are herein named 3rd-order Bresse circles.

Since the pattern is maintained also for n^{th}-order kinematic analysis, with the term n^{th}-order Bresse circles are herein denoted the loci of moving points with zero normal and tangential n^{th}-order kinematic characteristics. Consequently, the terminology 4th-order Bresse circles denotes the loci of moving points with zero tangential and normal jounce.

This paper is organized by analyzing in sequence, the n^{th}-order poles and Bresse circles, along with their applications to a four-bar, an offset slider-crank and a swinging block mechanism, respectively. Consequently, specific kinematic properties of n^{th}-order Bresse circles are presented and proven for the first time in the form of three novel theorems, by means of the proposed formulation, which has been validated by significant graphical and numerical results for several crank-driven four-bar mechanisms in different configurations. Moreover, the proposed algorithm allows to analyze the kinematic performance of different crank-driven four-bar mechanisms, the dwell configurations included, which are useful to design long-dwell mechanisms by using the dead-points superposition method, as first proposed in [6].

2. Nth-order poles: crank-driven rigid body

A generic crank-driven rigid body in planar motion is considered by referring to the sketch of Fig. 1, where the driving crank A_0A trasmists the motion to the point A, in terms of angular position θ_2, velocity ω_2, acceleration α_2 and jerk β_2, while the corresponding

[1] We observe that the velocity pole P_1 does not belong to the zero normal acceleration or inflection circle.
[2] We observe that the velocity pole P_1 does not belong to the zero-normal jerk circle.

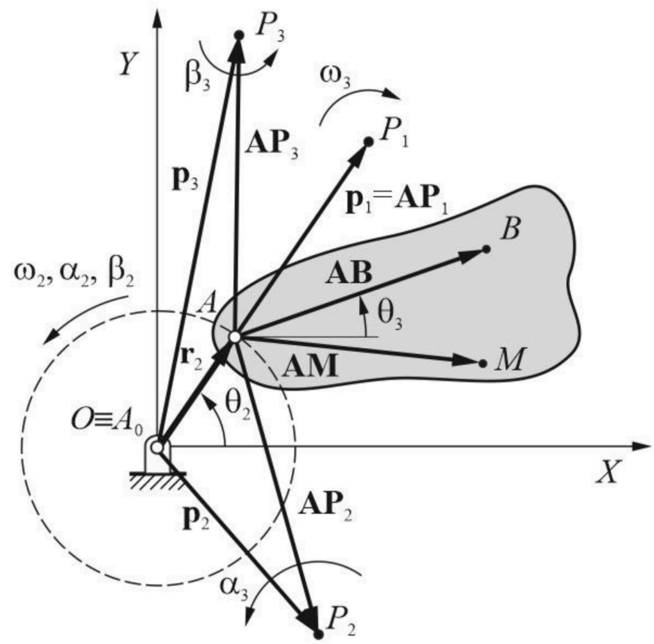

Fig. 1. Crank-driven rigid body in planar motion.

angular rotation θ_3, velocity ω_3, acceleration α_3 and jerk β_3 of the coupler plane, are supposed to be assigned.

Consequently, the position **OB**, velocity $\mathbf{v}_B$, acceleration $\mathbf{a}_B$ and jerk $\mathbf{J}_B$ vectors of point B of the coupler-link AB that sketches the coupler plane, can be determined, as follows

$$\mathbf{OB} = \mathbf{r}_2 + \mathbf{AB} \tag{1}$$

$$\mathbf{v}_B = \dot{\mathbf{r}}_2 + \boldsymbol{\omega}_3 \times \mathbf{AB} \tag{2}$$

$$\mathbf{a}_B = \ddot{\mathbf{r}}_2 + \boldsymbol{\alpha}_3 \times \mathbf{AB} + \boldsymbol{\omega}_3 \times (\boldsymbol{\omega}_3 \times \mathbf{AB}) \tag{3}$$

$$\mathbf{J}_B = \dddot{\mathbf{r}}_2 - \boldsymbol{\omega}_3^2(\boldsymbol{\omega}_3 \times \mathbf{AB}) - 3\boldsymbol{\omega}_3\boldsymbol{\alpha}_3 \cdot \mathbf{AB} + \dot{\boldsymbol{\alpha}}_3 \times \mathbf{AB} \tag{4}$$

where, correspondingly, for the point A and in Cartesian form with respect to the fixed frame Oxy, one have these expressions

$$\mathbf{r}_2 = (r_2\cos\theta_2)\mathbf{i} + (r_2\sin\theta_2)\mathbf{j} \tag{5}$$

$$\mathbf{v}_A = \dot{\mathbf{r}}_2 = -(\omega_2 r_2 \sin\theta_2)\mathbf{i} + (\omega_2 r_2\cos\theta_2)\mathbf{j} \tag{6}$$

$$\mathbf{a}_A = \ddot{\mathbf{r}}_2 = \left(-\omega_2^2 r_2\cos\theta_2 - \alpha_2 r_2\sin\theta_2\right)\mathbf{i} + \left(-\omega_2^2 r_2\sin\theta_2 + \alpha_2 r_2\cos\theta_2\right)\mathbf{j} \tag{7}$$

$$\mathbf{J}_A = \dddot{\mathbf{r}}_2 = \left(-3\omega_2\alpha_2 r_2\cos\theta_2 - \left(\alpha_2 - \omega_2^3\right) r_2\sin\theta_2\right)\mathbf{i} + \left(-3\omega_2\alpha_2 r_2\sin\theta_2 + \left(\dot{\alpha}_2 - \omega_2^3\right) r_2\cos\theta_2\right)\mathbf{j} \tag{8}$$

where $\mathbf{r}_2$ is the position vector of A and its first, second and third time derivatives are the velocity $\mathbf{v}_A$, acceleration $\mathbf{a}_A$ and jerk $\mathbf{J}_A$ vectors, respectively.

In particular, the position vectors $\mathbf{p}_1$, $\mathbf{p}_2$ and $\mathbf{p}_3$ of the velocity, acceleration and jerk poles P_1, P_2 and P_3 with zero -velocity, -acceleration and -jerk, respectively, can be determined by using the corresponding Rivals theorems, as follows

$$\mathbf{v}_{P1} = \dot{\mathbf{p}}_1 = \dot{\mathbf{r}}_2 + \boldsymbol{\omega}_3 \times \mathbf{AP}_1 \tag{9}$$

$$\mathbf{a}_{P2} = \ddot{\mathbf{p}}_2 = \ddot{\mathbf{r}}_2 + \boldsymbol{\alpha}_3 \times \mathbf{AP}_2 + \boldsymbol{\omega}_3 \times (\boldsymbol{\omega}_3 \times \mathbf{AP}_2) \tag{10}$$

$$\mathbf{J}_{P3} = \dddot{\mathbf{p}}_3 = \dddot{\mathbf{r}}_2 - \boldsymbol{\omega}_3^2(\boldsymbol{\omega}_3 \times \mathbf{AP}_3) - 3\boldsymbol{\omega}_3\boldsymbol{\alpha}_3 \cdot \mathbf{AP}_3 + \dot{\boldsymbol{\alpha}}_3 \times \mathbf{AP}_3 \tag{11}$$

by which, the following position vectors in Cartesian form, are obtained

$$\mathbf{p}_1 = \left(-\frac{\dot{r}_{2y}}{\omega_3} + r_{2x}\right)\mathbf{i} + \left(\frac{\dot{r}_{2x}}{\omega_3} + r_{2y}\right)\mathbf{j} \tag{12}$$

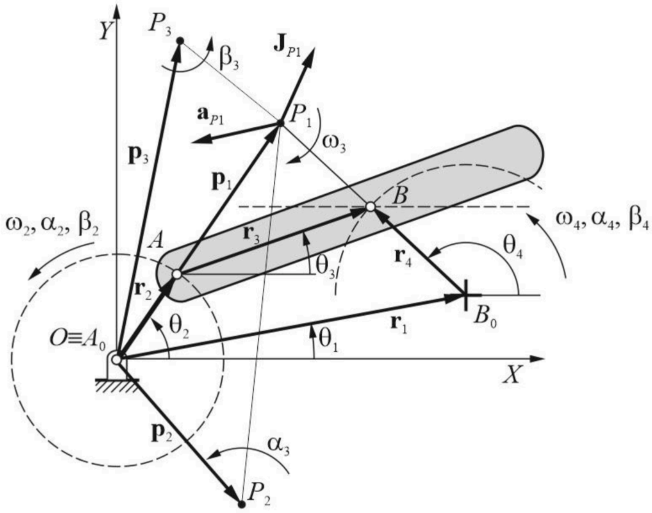

Fig. 2. Crank-driven four-bar linkage.

$$\mathbf{p}_2 = \left(r_{2x} - \frac{\ddot{r}_{2y}}{\alpha_3} + \frac{\omega_3^2}{\alpha_3}\,\frac{\alpha_3 \ddot{r}_{2x} + \omega_3^2 \ddot{r}_{2y}}{\omega_3^4 + \alpha_3^2} \right)\mathbf{i} + \left(r_{2y} + \frac{\alpha_3 \ddot{r}_{2x} + \omega_3^2 \ddot{r}_{2y}}{\omega_3^4 + \alpha_3^2} \right)\mathbf{j} \tag{13}$$

$$\mathbf{p}_3 = \left(r_{2x} + \frac{3\omega_3\alpha_3 \dddot{r}_{2x} + \left(\omega_3^3 - \beta_3\right)\dddot{r}_{2y}}{\left(3\omega_3\alpha_3\right)^2 + \left(\omega_3^3 - \beta_3\right)^2} \right)\mathbf{i} + \left(r_{2y} + \frac{\dddot{r}_{2y}}{3\omega_3\alpha_3} - \frac{3\omega_3\alpha_3 \dddot{r}_{2x} + \left(\omega_3^3 - \beta_3\right)\dddot{r}_{2y}}{\left(3\omega_3\alpha_3\right)^2 + \left(\omega_3^3 - \beta_3\right)^2}\,\frac{\left(\omega_3^3 - \beta_3\right)}{3\omega_3\alpha_3} \right)\mathbf{j} \tag{14}$$

as function of the angular velocity ω_3, acceleration α_3 and jerk β_3 of the coupler plane and the Cartesian components r_{2x} and r_{2y}, along with their first, second and third time derivatives.

The velocity and acceleration poles are usually known in planar kinematics, as the instantaneous center of rotation (ICR) and the accelerations center, but the word pole is here preferred, because we are dealing with the kinematic properties of higher-order.

In general, this approach is valid for determining the position vector of the n^{th}-order poles, since the Rivals theorem for the coupler plane is still valid for the higher-order kinematics.

3. N$^{\text{th}}$-order Bresse circles: crank-driven rigid body

Bresse circles consist of the well-known inflection and stationarity circles, which intersect at the instantaneous center of rotation (ICR) or velocity pole P_1, and at the acceleration center P_2 or acceleration pole. Conversely, jerk circles correspond to the geometric loci, which coupler points have zero-normal and zero-tangential acceleration, respectively. Jerk circles still intersect at the velocity pole and also at a third point, which is named jerk pole P_3.

In particular, the inflection circle $\mathscr{I}$ is the geometric locus of the coupler points, which show an inflection point in their paths and is always tangent to both centrodes at velocity pole P_1. Thus, referring to Fig. 1 and considering a generic point M of the coupler plane, the equation of inflection circle $\mathscr{I}$ can be conveniently obtained by imposing the following condition

$$\mathbf{v}_M \times \mathbf{a}_M = \mathbf{0} \tag{15}$$

which espresses the cross product of vectors $\mathbf{v}_M$ and $\mathbf{a}_M$ of point M, when it coincides with an inflection point of the coupler plane. Thus, developing and using the Rivals theorem, one has

$$(\dot{\mathbf{r}}_2 + \boldsymbol{\omega}_3 \times \mathbf{AM}) \times \left[\ddot{\mathbf{r}}_2 + \boldsymbol{\alpha}_3 \times \mathbf{AM} + \boldsymbol{\omega}_3 \times (\boldsymbol{\omega}_3 \times \mathbf{AM})\right] = \mathbf{0} \tag{16}$$

which gives the following algebraic equation

$$x^2 + y^2 + A_I x + B_I y + C_I = 0 \tag{17}$$

where, the coefficients A_I, B_I and C_I are given by

$$A_I = \frac{r_{2x}\left(\omega_3^2\omega_2 - 2\omega_3^3 + \omega_2^2\omega_3\right) + r_{2y}(\omega_3\alpha_2 - \omega_2\alpha_3)}{\omega_3^3} \tag{18}$$

$$B_I = \frac{r_{2x}(- \omega_3\alpha_2 + \omega_2\alpha_3) + r_{2y}\left(\omega_3^2\omega_2 - 2\omega_3^3 + \omega_2^2\omega_3\right)}{\omega_3^3} \tag{19}$$

$$C_I = \frac{r_{2x}(\omega_2 - \omega_3)\left[r_{2x}\left(\omega_2^2 - \omega_3^2\right) + r_{2y}(\alpha_2 + \alpha_3)\right] - r_{2y}(\omega_2 - \omega_3)\left[r_{2x}(\alpha_2 + \alpha_3) - r_{2y}\left(\omega_2^2 - \omega_3^2\right)\right]}{\omega_3^3} \tag{20}$$

The stationarity circle $\mathscr{S}$ or second Bresse circle is the geometric locus of the coupler points that have a pure normal acceleration, which equation can be conveniently obtained as

$$\mathbf{v}_M \cdot \mathbf{a}_M = 0 \tag{21}$$

which espresses the dot product of vectors $\mathbf{v}_M$ and $\mathbf{a}_M$ of point M, when it coincides with a point of the coupler plane with zero-tangential acceleration.

Thus, developing and using the Rivals theorem, one has

$$(\dot{\mathbf{r}}_2 + \boldsymbol{\omega}_3 \times \mathbf{AM}) \cdot \left[\ddot{\mathbf{r}}_2 + \boldsymbol{\alpha}_3 \times \mathbf{AM} + \boldsymbol{\omega}_3 \times (\boldsymbol{\omega}_3 \times \mathbf{AM})\right] = 0 \tag{22}$$

which gives the following algebraic equation

$$x^2 + y^2 + A_S x + B_S y + C_S = 0 \tag{23}$$

where, the coefficients A_S, B_S and C_S are given by

$$A_S = \frac{r_{2x}(\omega_2\alpha_3 + \omega_3\alpha_2 - 2\omega_3\alpha_3) + r_{2y}\left(\omega_2\omega_3^2 - \omega_2^2\omega_3\right)}{\omega_3\alpha_3} \tag{24}$$

$$B_S = \frac{r_{2x}\left(- \omega_2\omega_3^2 + \omega_2^2\omega_3\right) + r_{2y}(\omega_2\alpha_3 + \omega_3\alpha_2 - 2\omega_3\alpha_3)}{\omega_3\alpha_3} \tag{25}$$

$$C_S = \frac{r_{2x}(\omega_2 - \omega_3)\left[r_{2x}(\alpha_2 - \alpha_3) - r_{2y}\left(\omega_2^2 - \omega_3^2\right)\right] + r_{2y}(\omega_2 - \omega_3)\left[r_{2x}\left(\omega_2^2 - \omega_3^2\right) + r_{2y}(\alpha_2 - \alpha_3)\right]}{\omega_3\alpha_3} \tag{26}$$

The zero-normal jerk circle $\mathscr{J}_{\mathscr{N}}$ is the geometric locus of the coupler points with the normal component of the jerk vector equal to zero, which means that the velocity and jerk vectors are parallel between them, by which, one has

$$\mathbf{v}_M \times \mathbf{J}_M = \mathbf{0} \tag{27}$$

which espresses the cross product of vectors $\mathbf{v}_M$ and $\mathbf{J}_M$ of point M, when it coincides with a point of the coupler plane with zero-normal jerk.

Thus, developing and using the Rivals theorem, one has

$$(\dot{\mathbf{r}}_2 + \boldsymbol{\omega}_3 \times \mathbf{AM}) \times \left[\dddot{\mathbf{r}}_2 - \boldsymbol{\omega}_3^2(\boldsymbol{\omega}_3 \times \mathbf{AM}) - 3\boldsymbol{\omega}_3\boldsymbol{\alpha}_3 \cdot \mathbf{AM} + \boldsymbol{\beta}_3 \times \mathbf{AM}\right] = 0 \tag{28}$$

which gives the following algebraic equation

$$x^2 + y^2 + A_{J_N} x + B_{J_N} y + C_{J_N} = 0 \tag{29}$$

where, the coefficients A_{J_N}, B_{J_N} and C_{J_N} are given by

$$A_{J_N} = \frac{3r_{2x}\left(\omega_2\omega_3\alpha_2 + \omega_2\omega_3\alpha_3 - 2\omega_3^2\alpha_3\right) + r_{2y}\left[\omega_2^3\omega_3 + \omega_3\beta_2 - \omega_3\beta_3 + \omega_3^4 - \left(-\omega_3^3 + \beta_3\right)(\omega_2 - \omega_3)\right]}{3\omega_3^2\alpha_3} \tag{30}$$

$$B_{J_N} = \frac{r_{2x}\left[\left(-\omega_3^3 + \beta_3\right)(\omega_2 - \omega_3) - \omega_2^3\omega_3 - \omega_3\beta_2 + \omega_3\beta_3 - \omega_3^4\right] + 3r_{2y}\left(\omega_2\omega_3\alpha_2 + \omega_2\omega_3\alpha_3 - 2\omega_3^2\alpha_3\right)}{3\omega_3^2\alpha_3} \tag{31}$$

$$C_{J_N} = \frac{r_{2x}(\omega_2 - \omega_3)\left[3r_{2x}(\alpha_2\omega_2 - \alpha_3\omega_3) + r_{2y}\left(- \omega_2^3 + \omega_3^3 + \beta_2 - \beta_3\right)\right] - r_{2y}(\omega_2 - \omega_3)\left[r_{2x}\left(- \omega_2^3 + \omega_3^3 + \beta_2 - \beta_3\right) + 3r_{2y}(\alpha_2\omega_2 - \alpha_3\omega_3)\right]}{3\omega_3^2\alpha_3} \tag{32}$$

The zero-tangential jerk circle $\mathscr{J}_{\mathscr{T}}$ is the locus of the coupler points with a tangential component of the jerk vector equal to zero, which means that the velocity and jerk vectors are orthogonal between them, by which, one has

$$\mathbf{v}_M \cdot \mathbf{J}_M = 0 \tag{33}$$

which espresses the dot product of vectors $\mathbf{v}_M$ and $\mathbf{J}_M$ of point M, when it coincides with a point of the coupler plane with zero-tangential jerk.

Thus, developing and using the Rivals theorem, one has

$$\left(\dot{\mathbf{r}}_2 + \boldsymbol{\omega}_3 \times \mathbf{AM}\right) \cdot \left[\dddot{\mathbf{r}}_2 - \boldsymbol{\omega}_3^2(\boldsymbol{\omega}_3 \times \mathbf{AM}) - 3\boldsymbol{\omega}_3\boldsymbol{\alpha}_3 \cdot \mathbf{AM} + \boldsymbol{\beta}_3 \times \mathbf{AM}\right] = 0 \tag{34}$$

which gives the following algebraic equation

$$x^2 + y^2 + A_{J_T}x + B_{J_T}y + C_{J_T} = 0 \tag{35}$$

where, the coefficients A_{J_T}, B_{J_T} and C_{J_T} are given by

$$\begin{aligned} A_{J_T} = {} & \frac{r_{2x}\left[\left(\beta_3 - \omega_3^3\right)(\omega_2 - \omega_3) - \omega_2^3\omega_3 + \omega_3\beta_2 - \omega_3\beta_3 + \omega_3^4\right]}{\omega_3\left(\beta_3 - \omega_3^3\right)} + \\ & + \frac{3r_{2y}\left[-\omega_2\omega_3\alpha_2 + \omega_3^2\alpha_3 + \omega_3\alpha_3(\omega_2 - \omega_3)\right]}{\omega_3\left(\beta_3 - \omega_3^3\right)} \end{aligned} \tag{36}$$

$$\begin{aligned} B_{J_T} = {} & \frac{3r_{2x}\left[\omega_2\omega_3\alpha_2 + \omega_3^2\alpha_3 + \omega_3\alpha_3(\omega_2 - \omega_3)\right]}{\omega_3\left(\beta_3 - \omega_3^3\right)} + \\ & + \frac{r_{2y}\left[\left(\beta_3 - \omega_3^3\right)(\omega_2 - \omega_3) - \omega_2^3\omega_3 + \omega_3\beta_2 - \omega_3\beta_3 + \omega_3^4\right]}{\omega_3\left(\beta_3 - \omega_3^3\right)} \end{aligned} \tag{37}$$

$$\begin{aligned} C_{J_T} = {} & \frac{r_{2x}(\omega_2 - \omega_3)\left[r_{2x}\left(-\omega_2^3 + \omega_3^3 + \beta_2 - \beta_3\right) + 3r_{2y}(\alpha_2\omega_2 + \alpha_3\omega_3)\right]}{\omega_3\left(\beta_3 - \omega_3^3\right)} + \\ & + \frac{r_{2y}(\omega_2 - \omega_3)\left[3r_{2x}(\alpha_2\omega_2 - \alpha_3\omega_3) + r_{2y}\left(-\omega_2^3 + \omega_3^3 + \beta_2 - \beta_3\right)\right]}{\omega_3\left(\beta_3 - \omega_3^3\right)} \end{aligned} \tag{38}$$

Consequently, the acceleration pole P_2 is the intersection of the 1st-order Bresse circles, i.e. the inflection $\mathscr{I}$ and stationary $\mathscr{S}$ circles, while the jerk pole P_3 is the intersection of the 2nd-order Bresse circles, i.e. the zero-normal $\mathscr{J}_{\mathscr{N}}$ and zero-tangential $\mathscr{J}_{\mathscr{T}}$ jerk circles, where the first intersection is located at the velocity pole P_1 for both pairs of Bresse circles. In general, these properties of the Bresse circles are true for the n^{th}-order Bresse circles, since they intersect each other at the nth order pole, as in the case of the fourth and fifth order by giving the jounce or snap and the crackle poles, respectively.

4. Higher-order acceleration and path curvature analysis

The field of accelerations and higher-order accelerations, such as jerk and jounce, is completely defined by means of the kinematic analysis methods discussed in the previous sections and based on the n^{th}-order poles and n^{th}-order Bresse circles.

The previous capability allows the development of a new method to compute the radius of curvature ρ_e of the path trajectory evolute, as well as the radius of curvature ρ_{ee} of the path trajectory evolute of evolute. The usefulness of ρ_e and ρ_{ee} in many kinematic design tasks and also dynamic analyses of centriphugal dampers is well established [3]. Thus, the kinematic analysis methods herein discussed provide the basis of innovative tools. As it will be shown, once the kinematic state of a point has been characterized in terms of its acceleration, jerk and jounce, the higher-order differential properties of a point path can be computed.

Pennestrì and Cera presented in [3] different geometric methods for the computation of such differential properties, as well as a discussion of their use in some meaningful engineering tasks. For the acceleration $\mathbf{a}$ of any point, it is well known that

$$\mathbf{a} = \ddot{s}\hat{\boldsymbol{\tau}} + \frac{\dot{s}^2}{\rho}\hat{\mathbf{n}} \tag{39}$$

where: s is the point trajectory curvilinear abscissa; ρ is the point trajectory radius of curvature; $\hat{\boldsymbol{\tau}}$ and $\hat{\mathbf{n}}$are the unit vectors tangent and normal to the point trajectory, respectively; dots denote differentiation with respect to time.

From Eq. (39), one has

$$\frac{1}{\rho} = \frac{|\mathbf{a} \times \hat{\boldsymbol{\tau}}|}{\dot{s}^2} \tag{40}$$

where $\mathbf{v} = \dot{s}\hat{\boldsymbol{\tau}}$ is the point velocity vector. This standard operation we will be herein extended for the analysis of higher-order path curvature of any point on the plane.

The time derivative of Eq. (39) yields the jerk vector $\mathbf{j}$ of a point as follows

$$\mathbf{j} = \left(\dddot{s} - \frac{\dot{s}^3}{\rho^2}\right)\hat{\boldsymbol{\tau}} + \left(3\frac{\dot{s}\,\ddot{s}}{\rho} - \frac{\dot{s}^3}{\rho^3}\rho_e\right)\hat{\mathbf{n}} \tag{41}$$

where

$$\rho_e = \rho\frac{d\rho}{ds} \tag{42}$$

is the radius of curvature of the point path evolute.

Hence, from equation Eq. (41), one has

$$\rho_e = \left(3\frac{\dot{s}\,\ddot{s}}{\rho} \mp |\mathbf{j}\times\hat{\boldsymbol{\tau}}|\right)\frac{\rho^3}{\dot{s}^3} \tag{43}$$

where the minus (plus) sign is adopted when the product vectors $\mathbf{j}\times\hat{\boldsymbol{\tau}}$ and $\hat{\mathbf{n}}\times\hat{\boldsymbol{\tau}}$ have (do not have) the same orientation.

The time derivative of Eq. (41) yields the jounce vector J of a point as follows

$$\mathbf{J} = \left[\ddddot{s} - \frac{6\dot{s}^2\ddot{s}\rho^2 - 3\dot{s}^4\rho_e}{\rho^4}\right]\hat{\boldsymbol{\tau}} + \left[\frac{4\dddot{s}\,\dot{s} + 3\ddot{s}^2}{\rho} - 6\frac{\dot{s}^2\ddot{s}}{\rho} - 6\frac{\dot{s}^2\ddot{s}}{\rho^3}\rho_e - \frac{\dot{s}^4}{\rho^3}\left(1 - 3\frac{\rho_e^2}{\rho^2} + \frac{\rho_{ee}}{\rho}\right)\right]\hat{\mathbf{n}} \tag{44}$$

where

$$\rho_{ee} = \rho\frac{d\rho_e}{ds} \tag{45}$$

From equation Eq. (44), the following formula can deduced

$$\rho_{ee} = \left[\left(\frac{4\dddot{s}\,\dot{s} + 3\ddot{s}^2}{\rho} - 6\frac{\dot{s}^2\ddot{s}}{\rho} - 6\frac{\dot{s}^2\ddot{s}}{\rho^3}\rho_e\right) - \frac{\dot{s}^4}{\rho^3}\left(1 - 3\frac{\rho_e^2}{\rho^2}\right) \mp |\mathbf{J}\times\hat{\boldsymbol{\tau}}|\right]\frac{\rho^4}{\dot{s}^4} \tag{46}$$

where the minus (plus) sign is adopted when the product vectors $\mathbf{J}\times\hat{\boldsymbol{\tau}}$ and $\hat{\mathbf{n}}\times\hat{\boldsymbol{\tau}}$ have (do not have) the same orientation. The proposed formulas (43) and (46) do not require the knowledge of polodes geometry, but only the kinematic state of the point.

5. Crank-driven four-bar mechanisms

The crank-driven rigid body of Fig. 1 can be considered as a part of a generic four-bar mechanism, such as, the four-bar linkage, the offset slider-crank mechanism and the swinging-block mechanism. Thus, the angular rotation θ_3, velocity ω_3, acceleration α_3 and jerk β_3 of the coupler link AB, can be determined as function of the kinematic input data of the driving crank, which are the angular position θ_2, velocity ω_2, acceleration α_2 and jerk β_2, respectively. This is also true for the higher-order kinematics.

Therefore, applying the loop-closure equation to each of the above mentioned crank-driven mechanisms, a general algorithm is formulated in order to analyze the kinematic properties of n$^{\text{th}}$-order Bresse circles intersections.

5.1. Four-bar linkage

Referring to the crank-driven four-bar linkage of Fig. 2, the loop-closure equation is

$$\mathbf{r}_1 - \mathbf{r}_2 - \mathbf{r}_3 + \mathbf{r}_4 = \mathbf{0} \tag{47}$$

where vectors $\mathbf{r}_1$, $\mathbf{r}_2$, $\mathbf{r}_3$ and $\mathbf{r}_4$ can be expressed in general in Oxy, as

$$\begin{aligned}&\mathbf{r}_i = (r_i\cos\theta_i)\mathbf{i} + (r_i\sin\theta_i)\mathbf{j}\\ &i = 1,\ldots,n\end{aligned} \tag{48}$$

and for $n = 4$, r_2, r_3 and r_4 are the lengths of the crank A_0A, the coupler AB and the crank or rocker B_0B, respectively, while r_1 is the length of the fixed frame A_0B_0. The angles θ_1, θ_2, θ_3 and θ_4 give the angular position of vectors $\mathbf{r}_1$, $\mathbf{r}_2$, $\mathbf{r}_3$ and $\mathbf{r}_4$.

Thus, the angular position θ_3 of coupler link AB is given by

$$\theta_3 = \tan^{-1}\left(\frac{r_1\sin\theta_1 - r_2\sin\theta_2 + r_4\sin\theta_4}{r_1\cos\theta_1 - r_2\cos\theta_2 + r_4\cos\theta_4}\right) \tag{49}$$

and its time derivatives, up to the third order, give the angular velocity $\boldsymbol{\omega}_3$, acceleration $\boldsymbol{\alpha}_3$ and jerk $\boldsymbol{\beta}_3$ vectors, as follows

$$\boldsymbol{\omega}_3 = \dot{\theta}_3\,\mathbf{k} = \left(\omega_2 \frac{r_2}{r_3}\frac{\sin(\theta_2-\theta_4)}{\sin(\theta_4-\theta_3)}\right)\mathbf{k} \tag{50}$$

$$\boldsymbol{\alpha}_3 = \ddot{\theta}_3\,\mathbf{k} = \left(\frac{r_2\alpha_2\sin(\theta_2-\theta_4)+r_2\omega_2^2\cos(\theta_2-\theta_4)+r_3\omega_3^2\cos(\theta_3-\theta_4)-r_4\omega_4^2}{r_3\sin(\theta_4-\theta_3)}\right)\mathbf{k} \tag{51}$$

$$\boldsymbol{\beta}_3 = \dddot{\theta}_3\mathbf{k} = \left(-\frac{A_2+B_2\tan\theta_4}{r_3(\cos\theta_3\tan\theta_4-\sin\theta_3)}\right)\mathbf{k} \tag{52}$$

where the coefficients A_2 and B_2 are given by

$$\begin{aligned} A_2 = & -r_2\beta_2\sin\theta_2 + r_2\omega_2^3\sin\theta_2 + r_3\omega_3^3\sin\theta_3 - r_4\omega_4^3\sin\theta_4 - 3r_2\omega_2\alpha_2\cos\theta_2 + \\ & -3r_3\omega_3\alpha_3\cos\theta_3 + 3r_4\omega_4\alpha_4\cos\theta_4 \end{aligned} \tag{53}$$

$$\begin{aligned} B_2 = & \, r_2\beta_2\cos\theta_2 - r_2\omega_2^3\cos\theta_2 - r_3\omega_3^3\cos\theta_3 + r_4\omega_4^3\cos\theta_4 - 3r_2\omega_2\alpha_2\sin\theta_2 + \\ & -3r_3\omega_3\alpha_3\sin\theta_3 + 3r_4\omega_4\alpha_4\sin\theta_4 \end{aligned} \tag{54}$$

Likewise, the angular position θ_4 of driven link B_0B takes the form

$$\theta_4 = \tan^{-1}\frac{-B_1+\sigma\sqrt{B_1^2-C_1^2+A_1^2}}{C_1-A_1} \tag{55}$$

where σ is equal to ± 1 according to the assembly mode and its coefficients are given by

$$\begin{aligned} A_1 &= 2r_1r_4\cos\theta_1 - 2r_2r_4\cos\theta_2 \\ B_1 &= 2r_1r_4\sin\theta_1 - 2r_2r_4\sin\theta_2 \end{aligned} \tag{56}$$

$$C_1 = r_1^2 + r_2^2 + r_4^2 - r_3^2 - 2r_1r_2(\cos\theta_1\cos\theta_2 + \sin\theta_1\sin\theta_2) \tag{57}$$

The angular velocity vector $\boldsymbol{\omega}_4$ is given by

$$\boldsymbol{\omega}_4 = \dot{\theta}_4\,\mathbf{k} = \left(\frac{r_2\omega_2}{r_4}\frac{\sin(\theta_2-\theta_3)}{\sin(\theta_4-\theta_3)}\right)\mathbf{k} \tag{58}$$

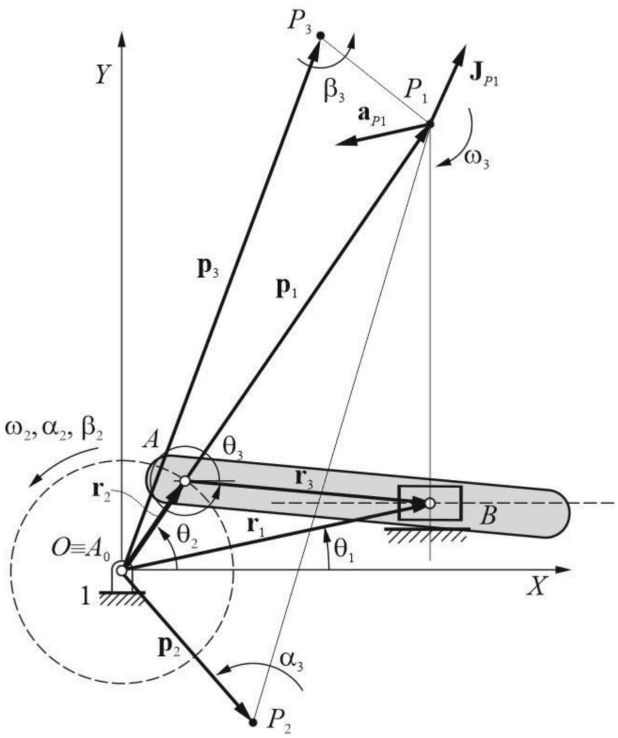

Fig. 3. Offset slider-crank mechanism.

and the angular acceleration vector $\boldsymbol{\alpha}_4$ takes the form

$$\boldsymbol{\alpha}_4 = \ddot{\theta}_4\,\mathbf{k} = \left(\frac{r_2\alpha_2\sin(\theta_2-\theta_3)+r_2\omega_2^2\cos(\theta_2-\theta_3)+r_3\omega_3^2-r_4\omega_4^2\cos(\theta_4-\theta_3)}{r_4\sin(\theta_4-\theta_3)}\right)\mathbf{k} \tag{59}$$

5.2. Offset slider-crank mechanism

Referring to the crank-driven offset slider-crank mechanism of Fig. 3, the angular position θ_3 of the coupler link *AB*, is given by

$$\theta_3 = \sin^{-1}\left(\frac{r_4 - r_2\sin\theta_2}{r_3}\right) \tag{60}$$

and its time derivatives, up to the third order, give the angular velocity $\boldsymbol{\omega}_3$, acceleration $\boldsymbol{\alpha}_3$ and jerk $\boldsymbol{\beta}_3$ vectors, as follows

$$\boldsymbol{\omega}_3 = \dot{\theta}_3\,\mathbf{k} = \left(-\frac{r_2\cos\theta_2}{r_3\cos\theta_3}\omega_2\right)\mathbf{k} \tag{61}$$

$$\boldsymbol{\alpha}_3 = \ddot{\theta}_3\,\mathbf{k} = \left(\frac{-\alpha_2 r_2\cos\theta_2+\omega_2^2 r_2\sin\theta_2+\omega_3^2 r_3\sin\theta_3}{r_3\cos\theta_3}\right)\mathbf{k} \tag{62}$$

$$\boldsymbol{\beta}_3 = \dddot{\theta}_3\mathbf{k} = \left(\frac{-\beta_2 r_2\cos\theta_2+\omega_2^3 r_2\cos\theta_2+3\omega_2\alpha_2 r_2\sin\theta_2+3\omega_3\alpha_3 r_3\sin\theta_3+\omega_3^3 r_3\cos\theta_3}{r_3\cos\theta_3}\right)\mathbf{k} \tag{63}$$

5.3. Swinging-block mechanism

Referring to the crank-driven swinging block mechanism of Fig. 4, the angular position θ_3 of the coupler link *AB*, is given by

$$\theta_3 = \tan^{-1}\left(\frac{-r_2\sin\theta_2}{s - r_2\cos\theta_2}\right) \tag{64}$$

and its time derivatives, up to the third order, give the angular velocity $\boldsymbol{\omega}_3$, acceleration $\boldsymbol{\alpha}_3$ and jerk $\boldsymbol{\beta}_3$ vectors, as follows

$$\boldsymbol{\omega}_3 = \dot{\theta}_3\,\mathbf{k} = \left(-\frac{r_2\omega_2}{r_3}(\sin\theta_2\tan\theta_3+\cos\theta_2)\cos\theta_3\right)\mathbf{k} \tag{65}$$

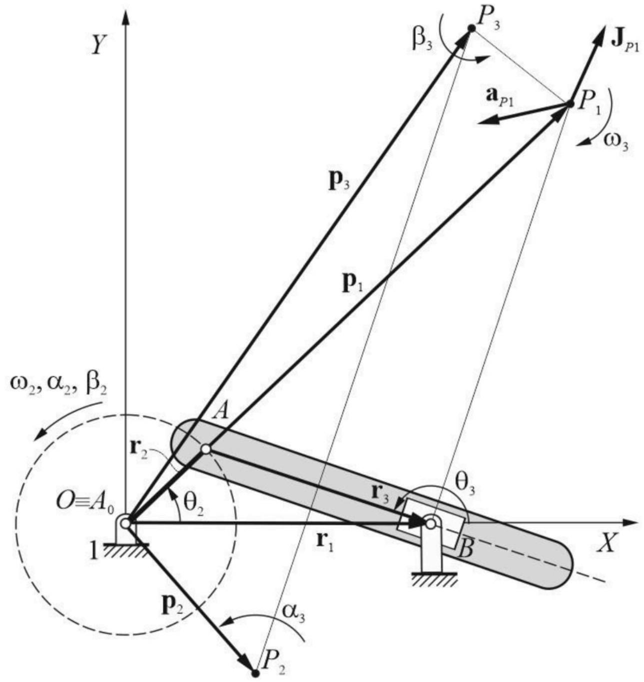

Fig. 4. Crank-driven swinging-block mechanism.

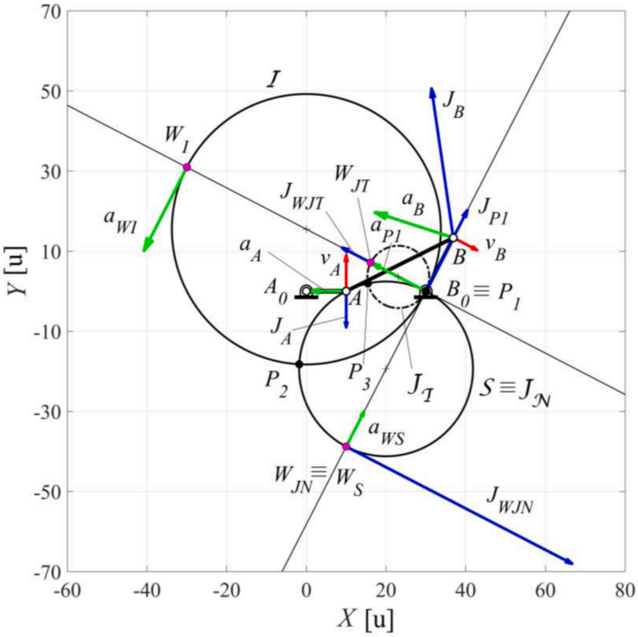

Fig. 5. Crank-driven four-bar linkage: Bresse and jerk circles, along with the velocity, acceleration and jerk vectors of points A, B and pole P_1, when $\theta_2 = 0^\circ$

$$\boldsymbol{\alpha}_3 = \ddot{\theta}_3\mathbf{k} = \left(\frac{\cos\theta_3}{r_3}(A_3\tan\theta_3 - B_3)\right)\mathbf{k} \tag{66}$$

$$\boldsymbol{\beta}_3 = \dddot{\theta}_3\mathbf{k} = \left(\frac{\cos\theta_3}{r_3}(A_4\tan\theta_3 - B_4)\right)\mathbf{k} \tag{67}$$

where

$$A_3 = -r_2\alpha_2\sin\theta_2 - r_2\omega_2^2\cos\theta_2 - 2\dot{r}_3\omega_3\sin\theta_3 - r_3\omega_3^2\cos\theta_3 \tag{68}$$

$$B_3 = r_2\alpha_2\cos\theta_2 - r_2\omega_2^2\sin\theta_2 + 2\dot{r}_3\omega_3\cos\theta_3 - r_3\omega_3^2\sin\theta_3 \tag{69}$$

$$\begin{gathered}A_4 = -r_2\beta_2\sin\theta_2 + r_2\omega_2^3\sin\theta_2 - 3r_2\omega_2\alpha_2\cos\theta_2 - 3\dot{r}_3\alpha_3\sin\theta_3 - 2\dot{r}_3\omega_3\sin\theta_3 - \ddot{r}_3\omega_3\sin\theta_3 + \\ -3\dot{r}_3\omega_3^2\cos\theta_3 + r_3\omega_3^3\sin\theta_3 - 3r_3\omega_3\alpha_3\cos\theta_3\end{gathered} \tag{70}$$

$$\begin{gathered}B_4 = r_2\beta_2\cos\theta_2 - r_2\omega_2^3\cos\theta_2 - 3r_2\omega_2\alpha_2\sin\theta_2 + 3\dot{r}_3\alpha_3\cos\theta_3 + 2\dot{r}_3\omega_3\cos\theta_3 + \ddot{r}_3\omega_3\cos\theta_3 + \\ -3\dot{r}_3\omega_3^2\sin\theta_3 - r_3\omega_3^3\cos\theta_3 - 3r_3\omega_3\alpha_3\sin\theta_3\end{gathered} \tag{71}$$

The magniture r_3 of the position vector $\mathbf{r}_3$ of link AB can be expressed as

$$r_3 = \pm\sqrt{s^2 + r_2^2 - 2sr_2\cos\theta_2} \tag{72}$$

and its time derivatives, up to the third order, are given by

$$\dot{r}_3 = \left(\frac{r_2\omega_2\sin\theta_2 + r_3\omega_3\sin\theta_3}{\cos\theta_3}\right) \tag{73}$$

$$\ddot{r}_3 = \left(\frac{r_3\alpha_3\sin\theta_3 - A_3}{\cos\theta_3}\right) \tag{74}$$

$$\dddot{r}_3 = \left(\frac{r_3\beta_3\sin\theta_3 - A_4}{\cos\theta_3}\right) \tag{75}$$

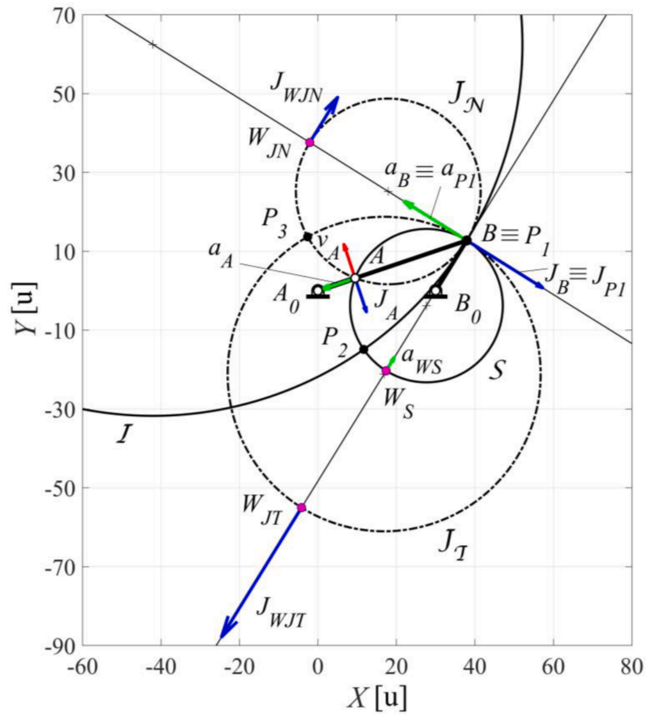

Fig. 6. - Crank-driven four-bar linkage: Bresse and jerk circles, along with the velocity, acceleration and jerk vectors of points *A, B* and pole P_1, when $\theta_2 = 18.575^\circ$

6. N$^{\text{th}}$-order Bresse circles intersections: kinematic properties

The position vector of center $O_{\mathscr{I}}$, radius $r_{\mathscr{I}}$ and diameter $\Delta_{\mathscr{I}}$ of the inflection circle $\mathscr{I}$ are respectively expressed by

$$\begin{aligned} \mathbf{O}_I &= \left(-\frac{A_I}{2}\right)\mathbf{i} + \left(-\frac{B_I}{2}\right)\mathbf{j} \\ r_I &= \sqrt{O_{Ix}^2 + O_{Iy}^2 - C_I} \\ \Delta_I &= 2r_I \end{aligned} \tag{76}$$

The position vector of inflection pole $W_{\mathscr{I}}$ is given by

$$\mathbf{W}_I = (2O_{Ix} - p_{1x})\mathbf{i} + \left(2O_{Iy} - p_{1y}\right)\mathbf{j} \tag{77}$$

The position vector of center $O_{\mathscr{J_N}}$, radius $r_{\mathscr{J_N}}$ and diameter $\Delta_{\mathscr{J_N}}$ of the zero-normal jerk circle $\mathscr{J}_{\mathscr{N}}$ are respectively, expressed by

$$\begin{aligned} \mathbf{O}_{J_N} &= \left(-\frac{A_{J_N}}{2}\right)\mathbf{i} + \left(-\frac{B_{J_N}}{2}\right)\mathbf{j} \\ r_{J_N} &= \sqrt{O_{J_N x}^2 + O_{J_N y}^2 - C_{J_N}} \\ \Delta_{J_N} &= 2r_{J_N} \end{aligned} \tag{78}$$

The position vector of zero-normal jerk pole $W_{\mathscr{J_N}}$ is given by

$$\mathbf{W}_{J_N} = (2O_{J_N x} - p_{1x})\mathbf{i} + \left(2O_{J_N y} - p_{1y}\right)\mathbf{j} \tag{79}$$

The magnitude of the acceleration vector $\mathbf{a}_{P1}$ is independent by the angular acceleration α_3 and can be expressed by

$$a_{P1} = \omega_3^2 \Delta_I \tag{80}$$

The magnitude of the acceleration vector $\boldsymbol{a}_{W_I}$ is independent of the angular velocity ω_3 and can be expressed by

$$a_{W_I} = \alpha_3 \Delta_I \tag{81}$$

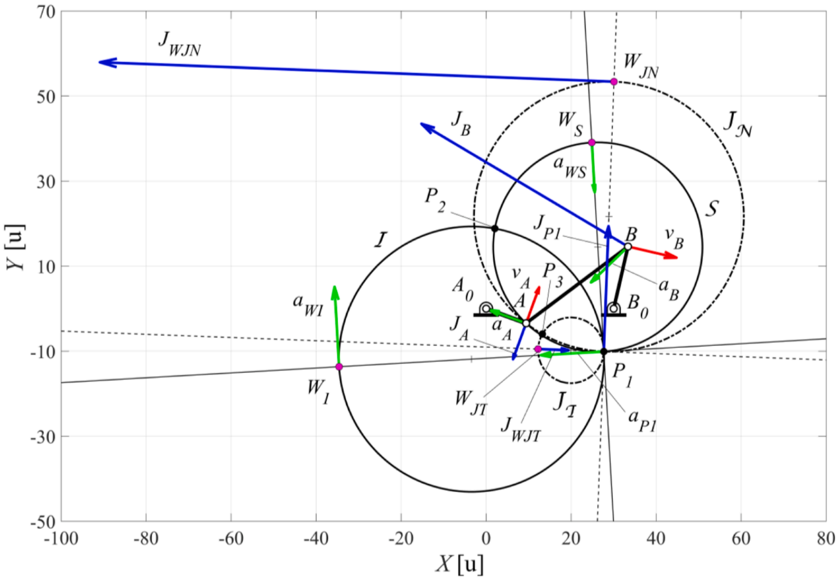

Fig. 7. - Crank-driven four-bar linkage: Bresse and jerk circles, along with the velocity, acceleration and jerk vectors of points *A, B* and pole P_1, when $\theta_2 = 340°$

Table 1
– Input data for a crank-driven four-bar linkage, (Dimensions in *u* unit length).

Example	r_1 [u]	r_2 [u]	r_3 [u]	r_4 [u]	θ_2 [deg]	ω_2 [r/s]	α_2 [r/s^2]	β_2 [r/s^3]
Fig. 5	30	10	30	15	0	1	0	0
Fig. 6	30	10	30	15	18.575°	1	0	0
Fig. 7	20	10	30	15	340°	1	0	0

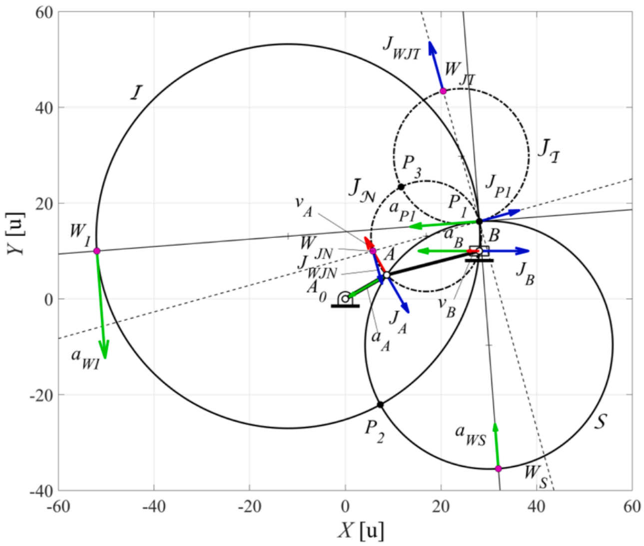

Fig. 8. Offset slider-crank mechanism: Bresse and jerk circles, along with the velocity, acceleration and jerk vectors of points *A, B* and pole P_1, when $\theta_2 = 30°$

The magnitude of jerk vector $\mathbf{J}_{P1}$ is independent of the angular jerk β_3 and can be expressed by

$$J_{P1} = 3\omega_3\alpha_3\Delta_{J_N} \tag{82}$$

The jerk $J_{W_{J_N}}$ of the zero-normal jerk pole $W_{\mathcal{J}\mathcal{N}}$ is independent of the angular acceleration α_3 and can be expressed by

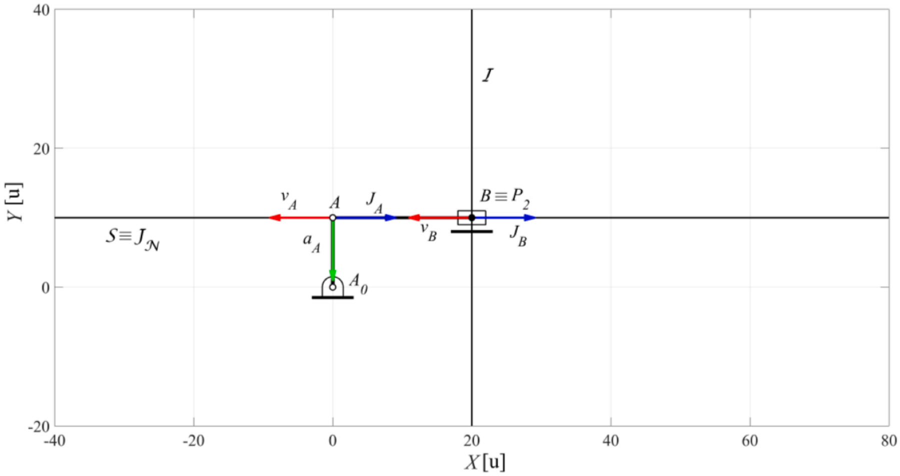

Fig. 9. - Offset slider-crank mechanism: Bresse and jerk circles, along with the velocity, acceleration and jerk vectors of points *A, B* and pole P_1, when $\theta_2 = 90^\circ$

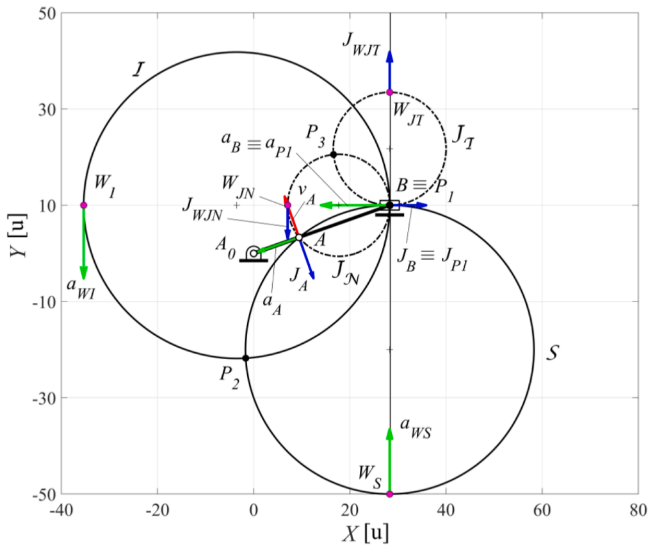

Fig. 10. - Offset slider-crank mechanism: Bresse and jerk circles, along with the velocity, acceleration and jerk vectors of points *A, B* and pole P_1, when $\theta = 19.47^\circ$

Table 2
– Input data for an offset slider-crank mechanism, (Dimensions in *u* unit length).

Example	e [u]	r [u]	l [u]	θ_2 [deg]	ω_2 [r/s]	α_2 [r/s^2]	β_2 [r/s^3]
Fig. 8	10	10	20	30°	1	0	0
Fig. 9	20	20	40	90°	1	0	0
Fig. 10	10	10	20	19.47°	1	0	0

$$J_{W_{J_N}} = \left(\omega_3^3 - \beta_3\right)\Delta_{J_N} \tag{83}$$

The acceleration vector $\mathbf{a}_{P1}$ of the velocity pole P_1 is parallel to $\overline{W_I P_1}$ and thus, one has

$$\mathbf{a}_{P1} \times \overline{W_I P_1} = \mathbf{0} \tag{84}$$

The jerk vector $\mathbf{J}_{P1}$ of the jerk pole P_1 is parallel to $\overline{W_{JN} P_1}$, and thus one has

$$\mathbf{J}_{P1} \times \overline{W_{JN} P_1} = \mathbf{0} \tag{85}$$

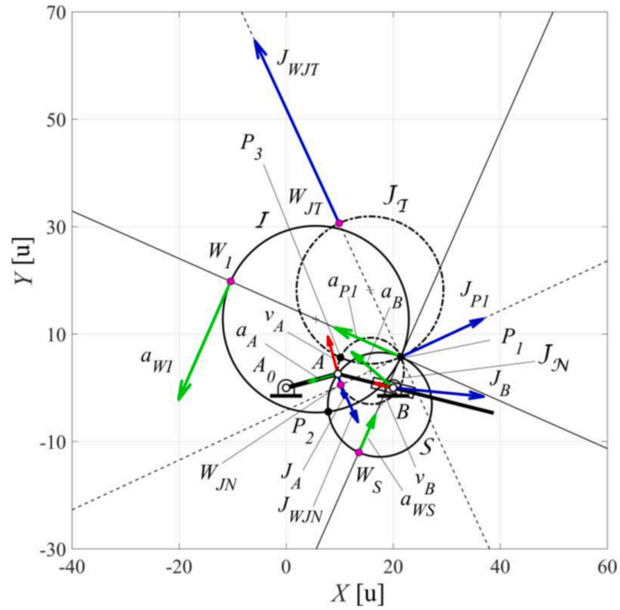

Fig. 11. Swinging-block mechanism: Bresse and jerk circles, along the velocity, acceleration and jerk vectors of points A, B and pole P_1, when $\theta_2 = 15°$

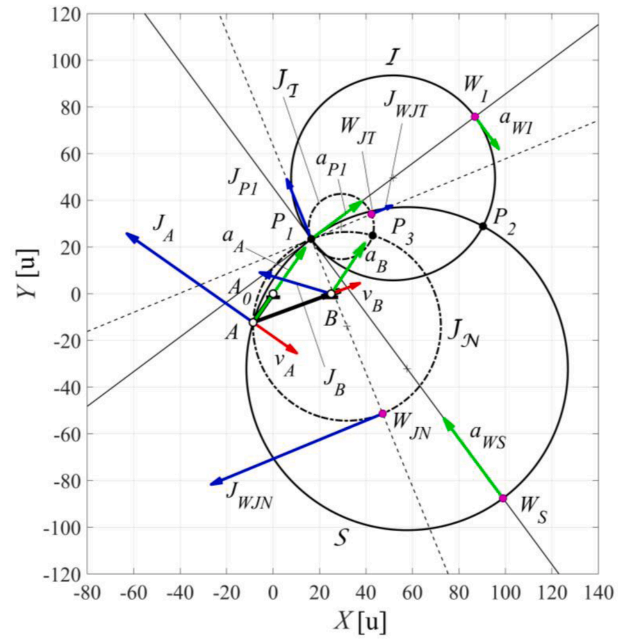

Fig. 12. Swinging-block mechanism: Bresse and jerk circles, along the velocity, acceleration and jerk vectors of points A, B and pole P_1, when $\theta_2 = 235°$

The angle γ_3 between the acceleration vector $\mathbf{a}_M$ of a generic coupler point M with respect the joining points P_2M is given by

$$\gamma_3 = \tan^{-1}\left(\frac{\alpha_3}{\omega_3^2}\right) \tag{86}$$

The angle λ_3 between the jerk vector $\mathbf{J}_M$ of a generic coupler point M with respect the joining points P_3M can be expressed by

$$\lambda_3 = \tan^{-1}\left(\frac{\omega_3^3 - \beta_3}{3\omega_3\alpha_3}\right) \tag{87}$$

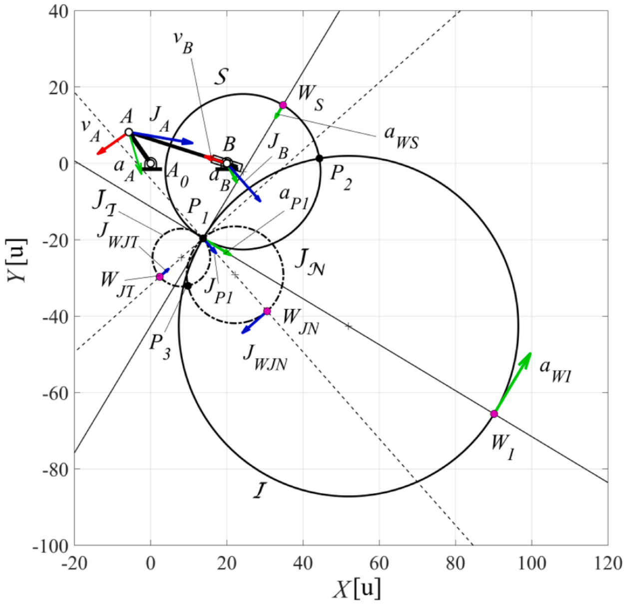

Fig. 13. Swinging-block mechanism: Bresse and jerk circles, along the velocity, acceleration and jerk vectors of points *A, B* and pole P_1, when $\theta_2 = 125°$

Table 3
– Input data for a swinging-block mechanism, (Dimensions in u unit length).

Example	r_1 [u]	r_2 [u]	θ_2 [deg]	ω_2 [r/s]	α_2 [r/s^2]	β_2 [r/s^3]
Fig. 11	20	10	15°	0.8	0	0
Fig. 12	25	15	235°	1.7	0	0
Fig. 13	20	10	125°	1.1	0.4	0

The magnitude of the acceleration vector $\mathbf{a}_M$ of a generic coupler point M is

$$a_M = \overline{P_2M}\sqrt{\omega_3^4 + \alpha_3^2} \tag{88}$$

The magnitude of the jerk vector $\mathbf{J}_M$ of a generic coupler point M can be expressed by

$$J_M = \overline{P_3M}\sqrt{\left(\omega_3^3 - \beta_3\right)^2 + \left(3\omega_3\alpha_3\right)^2} \tag{89}$$

Since the acceleration vector $\mathbf{a}_{W_I}$ of the inflection pole $W_{\mathscr{I}}$ is orthogonal to the acceleration vector $\mathbf{a}_{P1}$ of the velocity pole P_1, one has:

$$\mathbf{a}_{P1} \cdot \mathbf{a}_{W_I} = 0 \tag{90}$$

Thus, the acceleration vector $\mathbf{a}_{P1}$ is tangent to the stationarity circle $\mathscr{S}$, while the acceleration vector a_{W_I} is tangent to the inflection circle $\mathscr{I}$.

The jerk vector $\mathbf{J}_{W_{J_N}}$ of the zero-normal jerk pole $W_{\mathscr{J}\mathscr{N}}$ is orthogonal to the jerk vector $\mathbf{J}_{P1}$ of the velocity pole P_1, and thus, one has

$$\mathbf{J}_{P1} \cdot \mathbf{J}_{W_{J_N}} = 0 \tag{91}$$

and thus, the jerk vector $\mathbf{J}_{P1}$ is tangent to zero-tangential jerk circle $\mathscr{J}_{\mathscr{T}}$, while the jerk vector $\mathbf{J}_{W_{J_N}}$ is tangent to the zero-normal jerk circle $\mathscr{J}_{\mathscr{N}}$.

The Inflection circle $\mathscr{I}$ and stationarity circle $\mathscr{S}$ are orthogonal, and thus

$$\overline{O_IP_1}^2 + \overline{O_SP_1}^2 = \overline{O_IO_S}^2 \tag{92}$$

The zero-normal jerk circle $\mathscr{J}_{\mathscr{N}}$ and zero-tangential jerk circle $\mathscr{J}_{\mathscr{T}}$ are orthogonal, and thus

$$\overline{O_{JN}P_1}^2 + \overline{O_{JT}P_1}^2 = \overline{O_{JN}O_{JT}}^2 \tag{93}$$

The results of previous analysis allow to establish by induction the following theorems:

Theorem 1. *For a general planar motion, the loci of moving points with n^{th}-order ($n = 2,3,\ldots$) zero tangential and normal kinematic properties are orthogonally intersecting circles at pole velocity P_1 and n^{th}-order pole P_n. These circles are the n^{th}-order Bresse circles.*

Theorem 2. *The n^{th}-order kinematic property of pole velocity P_1 is independent of the angular n^{th}- order derivative and is always directed toward the pole, opposite to P_1, on the zero normal n^{th}-order Bresse circle.*

Theorem 3. *The n^{th}-order kinematic property of the pole opposite to P_1, on the zero normal n^{th}-order Bresse circle, is independent of the angular $(n-1)^{th}$- order derivative.*

7. Numerical examples

The Figs. 5–7 show the numerical and graphical results of a four-bar mechanism when the driving crank angle $\theta_2 = 0°$, $\theta_2 = 18.575°$and $\theta_2 = 340°$, respectively, along with the coupler curves, the velocity, acceleration and jerk vectors of points *A, B* and poles P_1, P_2 and P_3. The input data for the four-bar mechanism of Fig. 2 are reported in Table 1.

Figs. 8–10 show the numerical and graphical results of a slider-crank mechanism for the driving crank angle $\theta_2 = 30°$, $\theta_2 = 90°$ and $\theta_2 = \sin^{-1}\left(\frac{e}{r+l}\right)$=19.47°, respectively, along with the coupler curves, the velocity, acceleration and jerk vectors of points *A, B* and poles P_1, P_2 and P_3. The input data for the slider-crank mechanism of Fig. 3 are reported in Table 2.

The Figs. 11–13 show the numerical and graphical results of a swinging-block mechanism for the driving crank angle $\theta_2 = 15°$, $\theta_2 = 235°$ and $\theta_2 = 125°$, respectively, along with the coupler curves, the velocity, acceleration and jerk vectors of points *A, B* and poles P_1, P_2 and P_3. The input data for the swinging block mechanism of Fig. 4 are reported in Table 3.

8. Conclusions

The kinematic properties of the nth-order poles and Bresse circles intersections for a crank-driven rigid body, which belongs to a four-bar kinematic chain in the form of four-bar, slider-crank and swinging-block mechanisms, have been presented and proven by means of significant graphical and numerical results for different crank-driven four-bar mechanisms.

Moreover, three novel theorems dealing with the nth-order Bresse circles, which are orthogonally intersecting circles at pole velocity and nth-order pole, and the nth-order time-derivative position vectors of the velocity pole and its opposite point laying on the zero-normal nth-order Bresse circle, which is the inflection pole in the case of the zero-normal 2nd-order Bresse circle or inflection circle, have been formulated for the first time.

In particular, the first of these vectors is always oriented along the diameter of the zero-normal nth-order Bresse circle and has a magnitude that is independent of the angular nth-order derivative, while the second vector is always tangent to the same Bresse circle and has a magnitude that is independent of the angular $(n-1)^{th}$-order derivative.

Declaration of Competing Interest

The authors declare that they have no known competing financial interests or personal relationshi ps that could have appeared to influence the work reported in this paper.

Data availability

No data was used for the research described in the article.

References

[1] K.J. Waldron, G.L. Kinzel, S.K. Agrawal, Kinematics, Dynamics, and Design of Machinery, 3rd Edition, John Wiley & Sons Inc., ChichesterUK, 2016.
[2] A. Di Benedetto, E. Pennestrì, Introduzione Alla Cinematica dei Meccanismi, Vol. 1, 2, 3, Casa Editrice Ambrosiana, Milan, 1999 (in Italian).
[3] E. Pennestrì, M. Cera, Engineering Kinematics, Curvature theory of plane motion, 2023. (Available on Amazon).
[4] E.J. Routh, The Advanced Part of a Treatise on the Dynamics of a System of Rigid Bodies, Dover Publications, New York, 1955.
[5] G. Figliolini, P. Rea, J. Angeles, The pure-rolling cam-equivalent of the Geneva mechanism, Mech. Mach. Theory 41 (11) (2006) 1320–1335.
[6] G. Figliolini, C. Lanni, Jerk and jounce relevance for the kinematic performance of long-dwell mechanisms. Uhl T. (eds) Advances in Mechanism and Machine Science. IFToMM WC 2019. Mechanisms and Machine Science, 73, Springer, Cham, 2019, pp. 219–228.
[7] K.E. Özen, F.S. Dündar, M. Tosun, An alternative approach to jerk in motion along a space curve with applications, J. Theoret. Appl. Mech. 57 (2) (2019) 435–444.
[8] E. Hamouda, C. Cesarano, S. Askar, A. Elsharkawy, Resolutions of the jerk and snap vectors for a quasi curve in Euclidean 3-Space, Mathematics 9 (2021), 3128-16.
[9] A.M. Elshenhab, O. Moaaz, I. Dassios, A. Elsharkawy, Motion along a space curve with a quasi-frame in Euclidean 3-Space: acceleration and jerk, Symmetry (Basel) 14 (8) (2022) 1610–1615.
[10] J. Gallardo-Alvarado, J.M. Rico-Martinez, Jerk influence coefficients, via screw-theory, of closed chains, Meccanica 26 (2) (2001) 213–228.
[11] D. Condurache, Higher-order acceleration center and vector invariants of rigid body motion, in: Proc. of the 5th Joint Int. Conference on Multibody System Dynamics, Lisbon, Portugal, 2018. June 24-28paper n.160.
[12] D. Condurache, Higher-order kinematics of rigid bodies. A tensors algebra approach. Kecskeméthy A., Geu Flores F., Carrera E., Elias D. (eds), Interdisciplinary Applications of Kinematics. Mechanisms and Machine Science, 71, Springer, Cham, 2019.
[13] D. Stretti, P. Fanghella, G. Berselli, L. Bruzzone, Analytical expression of motion profiles with elliptic jerk, Robotica 41 (7) (2023) 1–15.

[14] W. Fan, X.S. Gao, W. Yan, C.M. Yuan, Interpolation of parametric CNC machining path under confined jounce, Int. J. Adv. Manuf. Technol. 62 (2012) 719–739.
[15] W. Steiner, On the impact of the jerk on structural dynamics, Proc. Appl. Math. Mech. 21 (2021) 1–3.
[16] J. Van Dam, K. Tanous, M. Werner, J.L. Gabbard, Calculating and analyzing angular head jerk in augmented and virtual reality: effect of AR cue design on angular Jerk, Appl. Sci. 11 (2021), 10082-13.
[17] A. Bresse, Mémoire sur un Théorème Nouveau Concernant Les Mouvements Plans et L'application de la Cinématique à la Détermination Des Rayons de Courbure, 20, J. de l'École Polytechnique, Paris, 1853, pp. 89–115.
[18] G.C. Steward, On the cardinal points in plane kinematics, philosophical transactions of the Royal Society of London, Ser. A: Math. Phys. Sci. 244 (875) (1951) 19–46.
[19] R.W. Schiller, Method for determining the instantaneous center of acceleration for a given link, J. Appl. Mech. 32 (1) (1965) 217–218.
[20] W. Meyer zur Capellen, G. Dittrich, Note on the determination of accelerations in plane kinematics, J. Mech. 1 (3) (1966) 315–319.
[21] H. Sun, T. Liu, Analysis of instantaneous center of zero acceleration of rigid body in planar motion, Modern Appl. Sci. 3 (4) (2009) 191–195.
[22] W.J. Carter, Second acceleration in four-bar mechanisms as related to rotopole, J. Appl. Mech. 25 (2) (1958) 293–294.
[23] C.H. Chiang, Graphical angular jerk analysis of four bar linkages, Mech. Mach. Theory 7 (4) (1972) 407–419.
[24] A. Kulkarni, D. Tesar, Properties of higher order instant center: a case study of classical motions, J. Mech. Robot. 5 (2) (2013) 024501–024514.
[25] N. Diab, A new graphical technique for acceleration analysis of four bar mechanisms using the instantaneous center of zero acceleration, SN Appl. Sci. 3 (2021) 327.
[26] G. Figliolini, L. Di Donato, R. Melloni, A.P. Bacchetta, C. Lanni, C. Preziosi, P. Rea, Mechatronic design of a robotic arm to remove skins by wine fermentation tanks, in: A. Carcaterra, A. Paolone, G. Graziani (Eds.), Proc. of XXIV AIMETA Conference 2019, eds, Lecture Notes in Mechanical Engineering. Springer, Cham, 2020, pp. 278–284.
[27] G. Figliolini, J. Angeles, The spherical equivalent of Bresse's circles: the case of crossed double-crank linkages, ASME J. Mech. Robot. 9 (1) (2017), 011014-11.
[28] G. Figliolini, C. Lanni, R. Kaur, Kinematic synthesis of spherical four-bar linkages for five-poses rigid body guidance. Uhl T. (eds), Advances in Mechanism and Machine Science. IFToMM WC 2019. Mechanisms and Machine Science, 2019, 73. Springer, Cham, pp. 639–648.
[29] B.J. Gilmore, R.J. Cipra, An analytical method for computing the instant centers, centrodes, inflection circles, and centers of curvature of the centrodes by successively grounding each link, J. Mech., Transm. Autom. 105 (3) (1983) 407–414.
[30] G. Figliolini, C. Lanni, Geometric loci for the kinematic analysis of planar mechanisms via the instantaneous geometric invariants. Gasparetto A., Ceccarelli M. (eds), Mechanism Design for Robotics. MEDER 2018. Mechanisms and Machine Science, 66, Springer, Cham, 2018, pp. 184–192.
[31] G. Figliolini, C. Lanni, M. Sorli, Kinematic analysis and centrodes between rotating tool with reciprocating motion and workpiece. Niola V., Gasparetto A., Quaglia G., Carbone G. (eds). Advances in Italian Mechanism Science. IFToMM Italy 2022. Mechanisms and Machine Science, 122, Springer, Cham, 2022, pp. 54–60.
[32] G. Figliolini, E. Pennestrì, Synthesis of quasi-constant transmission ratio planar linkages, ASME J. Mech. Des. 137 (10) (2015) 102301–102312.
[33] G. Figliolini, C. Lanni, L. Tomassi, First and second order centrodes of slider-crank mechanisms by using instantaneous invariants, in: O. Altuzarra, A. Kecskeméthy (Eds.), Proceeding in Advanced Robotics. ARK 2022. 18th International Symposium on Advances in Robot Kinematics, eds., Springer, 2022, pp. 303–310, 24 SPAR.
[34] G. Figliolini, C. Lanni, L. Tomassi, Kinematic analysis of slider – crank mechanisms via the Bresse and jerk's circles, in: A. Carcaterra, A. Paolone, G. Graziani (Eds.), Proceeding of XXIV AIMETA 2019, eds, Lecture Notes in Mechanical Engineering. Springer, Cham, 2020, pp. 278–284.